Blue light–excited LOV1 and LOV2 domains cooperatively regulate the kinase activity of full-length phototropin2 from *Arabidopsis*

Received for publication, October 10, 2017, and in revised form, November 15, 2017 Published, Papers in Press, December 1, 2017, DOI 10.1074/jbc.RA117.000324

Mao Oide[‡§], Koji Okajima[‡§1], Hirofumi Nakagami[¶‖], Takayuki Kato[**], Yuki Sekiguchi[‡§], Tomotaka Oroguchi[‡§], Takaaki Hikima[§], Masaki Yamamoto[§], and Masayoshi Nakasako[‡§]

From the [‡]Department of Physics, Faculty of Science and Technology, Keio University, 3-14-1 Hiyoshi, Kohoko-ku, Yokohama, Kanagawa 223-8522, Japan, [§]RIKEN SPring-8 Center, 1-1-1 Kouto, Sayo-cho, Sayo-gun, Hyogo 679-5148, Japan, [¶]RIKEN Center for Sustainable Resource Science, Yokohama 230-0045, Japan, [‖]Max Planck Institute for Plant Breeding Research, 50829 Cologne, Germany, and [**]Graduate School of Frontier Biosciences, Osaka University, 1-3 Yamadaoka, Suita, Osaka 565-0871, Japan

Edited by Joseph M. Jez

Phototropin2 (phot2) is a blue-light (BL) receptor that regulates BL-dependent activities for efficient photosynthesis in plants. phot2 comprises two BL-receiving light-oxygen-voltage–sensing domains (LOV1 and LOV2) and a kinase domain. BL-excited LOV2 is thought to be primarily responsible for the BL-dependent activation of the kinase. However, the molecular mechanisms by which small BL-induced conformational changes in the LOV2 domain are transmitted to the kinase remain unclear. Here, we used full-length wild-type and mutant phot2 proteins from *Arabidopsis* to study their molecular properties in the dark and under BL irradiation. Phosphorylation assays and absorption measurements indicated that the LOV1 domain assists the thermal relaxation of BL-excited LOV2 and vice versa. Using small-angle X-ray scattering and electron microscopy, we observed that phot2 forms a dimer and has a rod shape with a maximum length of 188 Å and a radius of gyration of 44 Å. Under BL, phot2 displayed large conformational changes that bent the rod shape. By superimposing the crystal structures of the LOV1 dimer, LOV2, and a homology model of the kinase to the observed changes, we inferred that the BL-dependent change consisted of positional shifts of both LOV2 and the kinase relative to LOV1. Furthermore, phot2 mutants lacking the photocycle in LOV1 or LOV2 still exhibited conformational changes under BL, suggesting that LOV1 and LOV2 cooperatively contribute to the conformational changes that activate the kinase. These results suggest that BL-activated LOV1 contributes to the kinase activity of phot2. We discuss the possible intramolecular interactions and signaling mechanisms in phot2.

Phototropin (phot)[2] is a blue-light (BL) receptor protein diversely present in green algae to land plants and is involved in the adaptation of organisms for efficient photosynthesis (1). In *Chlamydomonas reinhardtii* (Cr), phot mediates feedback regulation of photosynthesis through gene expression (2). In land plants, phototropism (3, 4), chloroplast movement (5, 6), stomata opening (7), and leaf expansion (8) are known as photomediated responses. Most higher plants have two isoforms of phot, designated as phot1 and phot2. phot1 and phot2 are activated by BL redundantly to regulate stomata opening, phototropism, and the accumulation of chloroplasts. The avoidance response of chloroplasts under high-fluence irradiation is mediated by only phot2 (5). phot1 and phot2 have different sensitivities to BL intensity; phot1 works in a broad range of BL intensities, whereas phot2 acts as a photoreceptor activated under high-fluence irradiation (4).

Phot proteins comprise ~1000 amino acid residues and two flavin mononucleotide (FMN) molecules and fold into three functional domains: two light-oxygen-voltage domains (LOV1 and LOV2) in the N-terminal half and one serine/threonine kinase domain (STK) in the C-terminal half (1) (Fig. 1*A*). LOV, which belongs to the Per-Arnt-Sim superfamily (9, 10), noncovalently binds one FMN molecule in a pocket formed by a characteristic tertiary structure named the α/β-scaffold (11, 12). The STK is classified into group VIII of the AGC protein kinase family and is expected to have a tertiary structure similar to protein kinase A (13).

Upon blue-light excitation, each LOV domain in the dark state (D_{450} state) undergoes a characteristic photocycle, and then the FMN transiently forms a covalent bond with a well-conserved cysteine residue in LOV (S_{390} state) (14–16). In phot2, the cysteine residues are Cys-170 in LOV1 and Cys-426 in LOV2. This local structural change induces a reorganization

This work was supported by Japan Society for the Promotion of Science (JSPS) Grants jp16H02218, jp22244054, jp22018027, jp20050030, jp1920402 (to M. N.), jp26800227, jp17H04854 (to T. O.), jp16K14682 (to T. K.), and jp15K18559 (to K. O.) and by Ministry of Education, Culture, Sports, Science and Technology (MEXT) Grants jp15076210, jp15H01647, jp17H05891, jp25120725, jp23120525 (to M. N.), and jp26104535 (to T. O.). The authors declare that they have no conflicts of interest with the contents of this article.

This article contains Fig. S1.

[1] To whom correspondence should be addressed: Dept. of Physics, Faculty of Science and Technology, Keio University, 3-14-1 Hiyoshi, Kohoko-ku, Yokohama, Kanagawa 223-8522, Japan. Tel.: 81-45-566-1713; Fax: 81-45-566-1672; E-mail: okajima@phys.keio.ac.jp.

[2] The abbreviations used are: phot, phototropin; At, *A. thaliana*; Cr, *C. reinhardtii*; BL, blue light; D_{450}, dark state; dark1, dark state 1 in small-angle X-ray scattering experiment; dark2, dark state 2 in small-angle X-ray scattering experiment; light1, state under blue light irradiation in small-angle X-ray scattering; LOV, light-oxygen-voltage–sensing domain; S_{390}, adduct state; SAXS, small-angle X-ray scattering; STK, serine/threonine kinase domain; SEC, size-exclusion column chromatography; λPPase, λ-protein phosphatase; R_g, radius of gyration.

of hydrogen bonds around the chromophore (17). The adduct form thermally reverts to the D_{450} state with a time constant from seconds to minutes in the dark (16). The phosphorylation activity of STK is enhanced by the small conformational changes of LOV2 in the S_{390} state (18). Therefore, LOV2 acts as the major regulator and forms a minimum functional unit with STK (LOV2-STK) (19, 20). Regarding the regulation of STK activity by BL-activated LOV2, unfolding and conformational changes of the Jα-helix, which associates with the C-terminal lateral region of the α/β-scaffold of LOV2, is critical for the intramolecular signaling (21). BL-activated phot displays autophosphorylation (19) and further phosphorylates substrate proteins, such as ATP-binding cassette subfamily B19 (22), phytochrome kinase substrate 4 (23), and blue-light signaling 1 (24), in the downstream part of the signaling pathway. Therefore, phot is a converter of BL stimuli to phosphorylation signals that activate signal transduction cascades, which induce the BL responses of plants.

Our structural study on LOV2-STK of *Arabidopsis thaliana* (At) phot2 (25) as a minimum functional unit revealed that LOV2 and STK are in a tandem arrangement and display rearrangements under BL irradiation. Similar conformational changes were observed in Crphot (26) and LOV2-STK of Atphot1 (27). In addition, we identified certain amino acid residues that are critical for regulating the STK activity in the A′α/Aβ gap of the N-terminal region of LOV2 and in the linker region connecting LOV2 and STK in Atphot1 (28, 29).

The analyses of spectroscopy and kinase assays for LOV2-STKs of both Atphot1 and Atphot2 demonstrated that the fluence-dependent sensitivity of phot correlated with the recovery speed from S_{390} to D_{450}; faster recovery resulted in a lower sensitivity, whereas slower recovery resulted in higher sensitivity (30). In Crphot, the truncation of LOV1 induced an acceleration of the recovery of LOV2, suggesting that LOV1 worked as an enhancer for light perception (26). In phot proteins of land plants, LOV1 also contributes to the regulation of LOV2 and the kinase activity (19, 31). However, details of the molecular mechanism and intramolecular interactions remain unclear.

In this study, we established a large-scale preparation system to provide full-length Atphot2, which comprised all residues in the amino acid sequence, and characterized the molecular properties of the wild-type protein and its mutants in terms of their kinase activities, dark recovery kinetics, and molecular structures. We report the results of biochemical, spectroscopic, and structural studies using small-angle X-ray scattering (SAXS) and electron microscopy (EM) and discuss the regulatory mechanism of Atphot2.

Results

Preparation of phot2

Wild-type Atphot2 (WT) was overexpressed and prepared at a purity greater than 95% as examined by sodium dodecyl sulfate (SDS)-polyacrylamide gel electrophoresis (PAGE) (Fig. S1A). In addition, three mutants (C170A, C426A, and D720N) were prepared for biochemical assays. The C170A (C426A) mutant can bind one FMN molecule to the pocket of the α/β-scaffold of LOV1 (LOV2) but has lost the ability to form the S_{390} state in the photoreaction cycles of LOV1 (LOV2). D720N mutation results in the complete loss of the kinase activity of STK.

By size-exclusion column chromatography (SEC), the apparent molecular weight of the WT was estimated as ~220,000, indicating a dimeric form of WT in solution (Fig. S1B). The dark-adapted WT (D_{450} state) had absorption peaks at 474, 446, and 371 nm and a shoulder around 410 nm consistent with those of the LOV1-LOV2 fragment (19). The absorbance values at 273 and 446 nm in the dark state indicated that each subunit was associated with two FMN molecules. Under BL irradiation, the WT showed absorption changes of the LOV domains (Fig. 1*B*) as observed for the LOV1-LOV2 fragment (16).

Kinase activity and phosphorylation sites of phot2

The kinase activity of the purified WT was examined by an autophosphorylation assay with and without BL irradiation (Fig. 1*C*). The WT showed phosphorylation activity in the dark as observed both *in vivo* and *in vitro* (3, 19), and the kinase activity was significantly enhanced under BL. As expected, the D720A mutant displayed little phosphorylation. The C170A mutant showed BL-accelerated autophosphorylation activity as observed in the WT, whereas the C426A mutant displayed little autophosphorylation under BL.

In a gel-shift assay, the WT, just after purification, had an apparent molecular weight larger than those of the WT incubated with λ-protein phosphatase (λPPase; New England Biolabs) and the D720N mutant (Fig. 1*D*). This result implied that the purified WT would be phosphorylated during overexpression and purification. In fact, 25 phosphorylation sites were identified in the previous study of the *in vivo* autophosphorylation of Atphot2 (32).

Autophosphorylation sites in the N-terminal half of λPPase-treated phot2 in the dark and under BL irradiation were identified by mass spectrometry (MS) (Fig. 1*E*). No phosphorylation sites were detected in the N-terminal half of the D720N mutant used as a reference. The λPPase treatment dephosphorylated the WT except at Ser-284 located near the C terminus of LOV1. After incubation in the presence of ATP in the dark, λPPase-treated WT was phosphorylated at Ser-22. After BL irradiation for 1 h, an additional phosphorylation was identified at Ser-106, suggesting a BL-dependent conformational change around the N-terminal region of LOV1.

Photoconversion to S_{390} and dark reversion of C170A/D720N, C426A/D720N, and C170A/C426A/D720N mutants

In addition to the three single mutants described in the previous sections, two double mutants (C170A/D720N and C426A/D720N) and one triple mutant (C170A/C426A/D720N) were overexpressed and purified to study the influence of the photocycle of each LOV domain on the BL responses of phot2 (Fig. S1C). These mutants lack the kinase activity and are free from heterogeneity regarding phosphorylation, making them suitable for physicochemical measurements requiring homogeneity of specimens.

The conversion from D_{450} to S_{390} and the dark reversion of S_{390} to D_{450} were measured by ultraviolet (UV)-visible absorp-

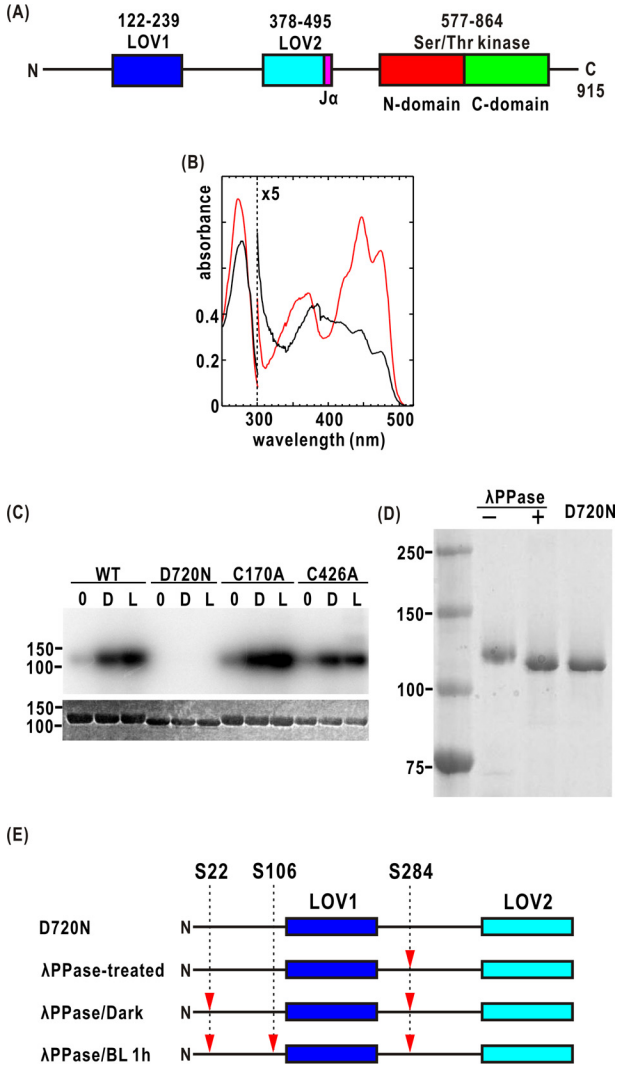

Figure 1. *A*, schematic illustration of the arrangement of LOV1, LOV2, Jα, and STK in the amino acid sequence of Atphot2. *B*, absorption spectra of D_{450} in the dark (*red line*) and under BL irradiation (*black line*) at a fluence of 200 μmol m^{-2} s^{-1}. The kink appearing at 380 nm was caused by the exchange of a filter. *C*, kinase assay of phot2 WT and its D720N, C170A, and C426A mutants. Labels "*0*," "*D*," and "*L*" indicate the specimens immediately after mixing, after 15-min incubation in the dark, and after 15-min incubation under BL, respectively. The *upper panel* shows an SDS-PAGE pattern taken using an imaging plate for the same gel stained by Coomassie Brilliant Blue (*lower panel*). *D*, result of a gel-shift assay for phot2 WT without and with λPPase treatment and D720N mutant. *E*, identification of phosphorylated residues in phot2 by MS. Schematics from the *top* to *bottom* are D720N mutant as a reference and WT specimens after λPPase treatment, after 1-h incubation of λPPase-treated in the dark, and after 1-h incubation of λPPase-treated under BL.

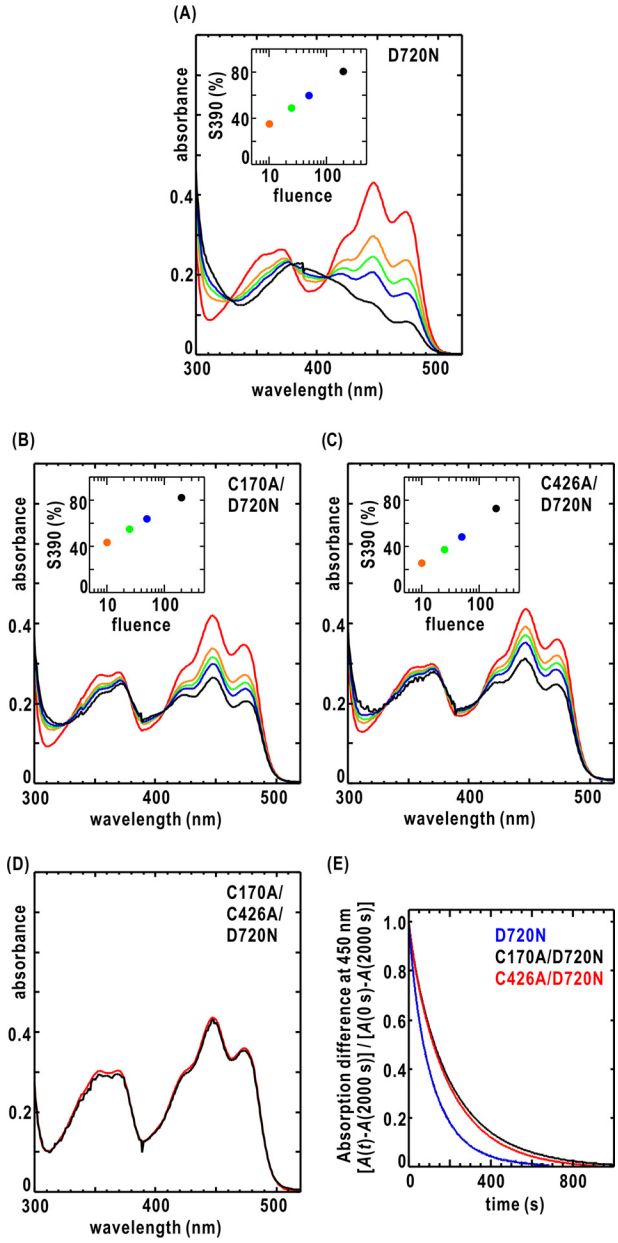

Figure 2. *A–C* show the absorption spectra of the D720N, C170A/D720N, and C426A/D720N mutants in the dark and under BL irradiation, respectively. D_{450} in the dark (*solid red line*) and under BL (λ_{max} = 460 nm) at a fluence of 10 (*orange*), 25 (*green*), 50 (*blue*), and 200 (*black*) μmol m^{-2} s^{-1} is shown. The *inset* shows the fluence-dependent accumulation of S_{390}. The accumulation ratio was calculated from the absorption change at 450 nm in the expected full conversion to S_{390} and that under BL irradiation. *D* shows the absorption spectra of C170A/C426A/D720N in the dark (*red*) and under BL irradiation (*black*) at a fluence of 200 μmol m^{-2} s^{-1}. *E*, dark reversion kinetics of S_{390} after turning off BL as monitored by the absorption change at 450 nm.

tion spectroscopy. The mutants were measured using SAXS as described below; therefore, they were suspended in the same buffer used in the SAXS experiments. In phot, the formation of S_{390} in LOV2 is essential (19), and the dark-reversion speed of S_{390} to D_{450} is one of the key factors for the activation of the kinase function (30). Both LOVs in the D720N mutant were almost completely converted to their S_{390} state under BL fluence at more than 450 μmol m^{-2} s^{-1} (Fig. 2*A*). BL irradiation at a fluence of 450 μmol m^{-2} s^{-1} converted more than 90% of C170A/D720N and C426A/D720N mutants to the S_{390} states of LOV2 and LOV1, respectively (Fig. 2, *B* and *C*). The triple mutant, prepared as a reference for the other three mutants, displayed little change in its absorption spectrum under BL irradiation (Fig. 2*D*).

Fig. 2*E* compares the dark reversion of C170A/D720N and C426A/D720N mutants with that of the D720 mutant. The dark-reversion kinetics of the D720N mutant was approximated by a double-exponential curve. The fast component, with a half-life time ($\tau_{1/2}$) of 54 s, corresponded to the dark reversion of LOV2, and the slow component, with a $\tau_{1/2}$ of 194 s, represented the reversion of LOV1. The dark reversion of LOV2 in the C170A/D720N mutant was approximated by a

single-exponential curve with a $\tau_{1/2}$ value of 168 s, which was approximately 3 times longer than that of LOV2 in the D720N mutant. These findings suggested a significant influence of LOV1 on the dark reversion of LOV2. In contrast, the dark reversion of LOV1 in the C426A/D720N mutant, which was approximated by a single-exponential curve with a $\tau_{1/2}$ value of 68 s, was faster than that of the D720N mutant. Mutual influences on the photocycles between LOV1 and LOV2 were suggested by the prolongation of the S_{390} lifetime of LOV2 in the C170A mutant and the acceleration of the dark reversion of LOV1 in the C426A mutant.

Molecular structure and BL-induced conformational changes of the D720N mutant

The low-resolution structure and BL-induced structural change of phot2 in solution were studied by SAXS for the D720N mutant because the heterogeneity of the phosphorylated WT and, probably, the phosphatase-treated WT was unsuitable for SAXS measurements. For each specimen solution, SAXS profiles were recorded in the dark (dark1), under BL at more than 450 μmol m^{-2} s^{-1} (light1), and again in the dark (dark2).

The scattering intensities of light1 increased in $S < 0.007$ $Å^{-1}$, whereas the profiles in the other regions remained almost the same (Fig. 3*A*). The intensity change in light1 at $S = 0.005$ $Å^{-1}$ corresponded to ~8% of the intensity of dark1. The profiles of dark2 resembled those of dark1, indicating that the BL-dependent SAXS changes were almost photoreversible (Fig. 3*A*, *inset*). These photoreversible SAXS changes were observed in the concentration range measured thus far.

The Guinier analysis (Fig. 3*B*) and the concentration dependences of the radius of gyration (R_g) and zero-angle scattering intensities (Fig. 3*C*) indicated that the specimen solutions were almost monodispersive (Fig. 4*C*). A dimeric association of the D720N mutant was confirmed from the apparent molecular weight estimated from the zero-angle scattering intensity. This finding was consistent with the result of SEC (Fig. S1B). The R_g values of dark1 (44.3 ± 1.4 Å) and dark2 (44.9 ± 1.4 Å) were comparable and slightly larger than that of light1 (43.7 ± 1.4 Å) (Fig. 3*C*). The R_g values were likely photoreversible as expected from the profiles. The distance distribution functions $P(r)$ of dark1, light1, and dark2, with shoulders at $r > 70$ Å, reflected their dimeric structures (Fig. 3*D*). The maximum dimensions were almost the same among dark1 (188 ± 2 Å), light1 (186 ± 2 Å), and dark2 (187 ± 2 Å).

The molecular shapes of dark1, light1, and dark2 were restored by the program GASBOR. The model shapes were multiply restored for each condition, and then the most probable shape was selected after classification of the restored molecular shapes using multivariate analyses (Fig. 4, *A* and *B*). The molecular shapes of dark1 and dark2 appeared as elongated Z-shapes with approximate dimensions of 185 Å long and 80 Å wide in the Z-shape view and 55 Å thick in the rod-shape view. The molecular model of light1 appeared with a Z-shape but had a bend around the center in the rod -shape view, indicating BL-induced conformational changes. The bend induced movements of both edges of the rod shape by ~30 Å.

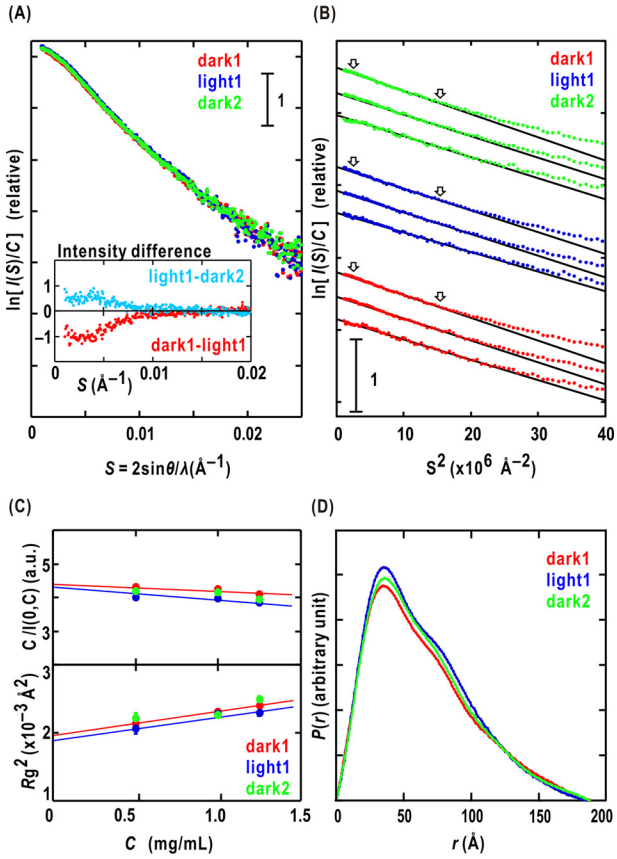

Figure 3. *A*, SAXS profiles of D720N mutant solution of 0.8 mg ml^{-1} in dark1 (*red dots*), light1 (*blue dots*), and dark2 (*green dots*). The *inset* shows difference SAXS profiles between dark1 and light1 (*magenta dots*) and between light1 and dark2 (*cyan dots*). *B*, Guinier plots, which show the dependence of the logarithm of the scattering intensity on the square of the scattering vector, for dark1, light1, and dark2 of the D720N mutant. For clarity, each plot is shifted along the *ordinate*. The concentrations from the *top* to *bottom* in each state were 1.2, 1.0, and 0.5 mg ml^{-1}, respectively. The least-squares fitting method was applied for the data in the region indicated by the *arrows* to calculate the $I(0)$ and R_g assuming the Guinier approximation. The high-resolution edges of the region ($S^2 = 15 \times 10^{-6}$ $Å^2$) satisfy the criteria for applying the approximation ($SR_g < (2\pi)^{-1}$). *C*, the concentration dependences of $C/I(0, C)$ (*upper panel*) and $R_g(C)^2$ (*lower panel*) values of dark1, light1, and dark2. For the $C/I(0, C)$ data, the standard deviations are smaller than the sizes of the symbols. *D*, $P(r)$ functions of the D720N mutant in the dark1, light1, and dark2. *a.u.*, arbitrary units.

Furthermore, the molecular shapes of the negatively stained C170A/C426A/D720N mutant were visualized by transmission electron microscopy. Although negative staining might induce conformational changes of C170A/C426A/D720N, molecular images and dimensions consistent with the SAXS models were observed (Fig. 4*C*), indicating that the model shapes predicted from the SAXS profiles would approximate the molecular shape of the D720N mutant.

BL-induced SAXS changes in the C170A/D720N and C426A/D720N mutants

Next, to understand which BL-activated LOV domain was responsible for the BL-induced conformational changes in the D720N mutant, SAXS of the C170A/D720N, C426A/D720N, and C170A/C426A/D720N mutants was measured in the dark and under BL irradiation (Fig. 4*E*). The three mutants were almost monodispersive and displayed profiles similar to that of D720N mutant in the dark (Fig. 3*D*). The magnitudes of the

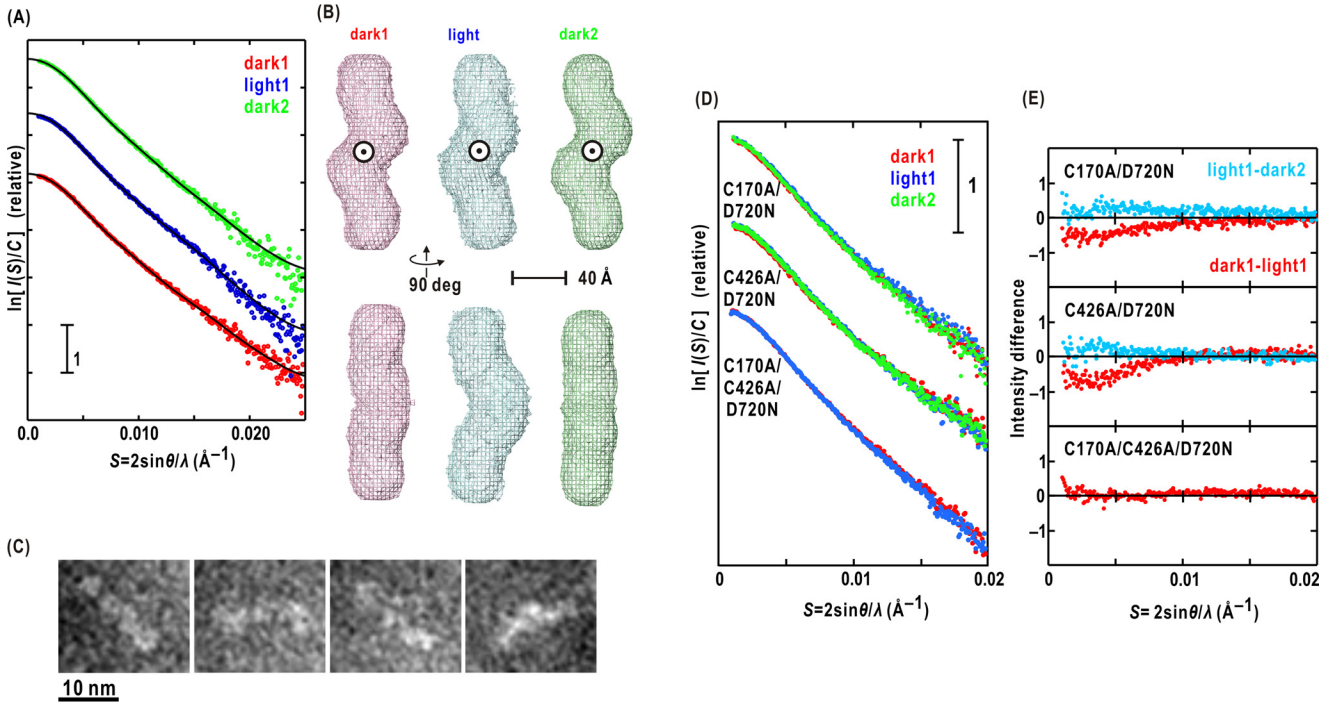

Figure 4. *A*, the SAXS profiles of the D720N mutant in dark1 (*red dots*), light1 (*blue dots*), and dark2 (*green dots*) states are compared with those calculated from their GASBOR models (*black*). For clarity, profiles plotted in semilogarithmic form are shifted appropriately along the *ordinate*. *B*, the molecular shapes of dark1 (*pink mesh*), light1 (*cyan mesh*), and dark2 (*green mesh*) are illustrated as density maps of dummy residues in $4 \times 4 \times 4$-Å^3 cubes after averaging a set of the most probable models. In the *lower panel*, the 2-fold symmetry axis is indicated on the model views rotated by 90° from the upper. *C*, typical images of C170A/C246A/D720N mutant viewed by EM. *D*, the SAXS profiles of the C170A/D720N, C426A/D720N, and C170A/C426A/D720N mutants in dark1 (*red dots*), light1 (*blue dots*), and dark2 (*green dots*). *E*, differences in the SAXS profiles of the three mutants between dark1 and light1 (*magenta dots*) and between light1 and dark2 (*cyan dots*).

differences in the SAXS profiles (dark1 − light1 and light1 − dark2) of both the C170A/D720N and C426A/D720N mutants were smaller than those of D720N mutant, even when taking into account the incomplete conversion of each LOV in C170A/D720N and C426A/D720N mutants (~90%). In contrast, the C170A/C426A/D720N mutant showed little change in SAXS and the absorption spectra (Fig. 2*D*). Therefore, both BL-excited LOV1 and LOV2 would induce the conformational changes detectable by SAXS in the C426A/D720N and C170A/D720N mutants, respectively. However, the magnitudes in the SAXS differences in the double mutants were smaller than those of the D720N mutant.

Discussion

The biochemical, spectroscopic, and structural studies on purified full-length phot2 and its mutants suggested a contribution of LOV1, as well as LOV2, to the kinase activity and BL-dependent conformational changes of Atphot2. Here, we discuss the implications of the results for the illustration of the molecular organization and intramolecular signaling to induce cellular signaling cascades in the BL response by phot2.

Domain organization and BL-induced conformational changes in Atphot2

The WT and mutants exist as dimers in solution as suggested by SEC, SAXS, and EM (Figs. S1B and 4, *B* and *C*). The molecular shape of dark1 (and dark2) of the D720N mutant was approximated by arranging the molecular models of the LOV1 dimer and monomeric LOV2-STK proposed in our previous studies (Fig. 5*A*). Considering the fact that LOV1 forms a dimer both in the crystal (33) and in solution (34), the LOV1 dimer probably acts as a dimerization site and occupies the central part of the molecular shape. Then the crystal structure of phot2 LOV2 (35) and a homology model of STK (25) were fitted to the edge lobes of the molecular shapes of dark1 and light1.

Under BL, the LOV1 dimer exhibited little conformational change when viewed at a low resolution (34). In addition, LOV2-STK exhibits BL-induced rearrangement of LOV2 relative to STK. Therefore, the global changes in the molecular shape under BL would be mainly attributed to the BL-induced rearrangement of LOV2 and STK observed in Atphot2 LOV2-STK (25) (Fig. 5*A*). Most of the phosphorylation sites identified in the N-terminal half of Atphot2 (32) are far from the active site of STK in the model of light1; therefore, those sites would be phosphorylated by other phot2 dimers. In contrast, Ser-22, which is located in the edge of the long N-terminal tail composed of ~100 amino acid residues (Fig. 1*A*), might reach the active-site cleft of STK to be self-phosphorylated.

To ensure the homogeneity of specimens in physicochemical measurements, we studied kinase-inactivated mutants. However, phosphorylation may still have certain effects on BL-induced structural changes in wild-type phot2. For investigating the influences of phosphorylation on conformational changes, purification techniques to separate wild-type phot2 at different phosphorylation levels will be necessary in the future.

In crude extract of wild-type phot2 under BL, more than 25 phosphorylation sites were found (32). In contrast, in the *in*

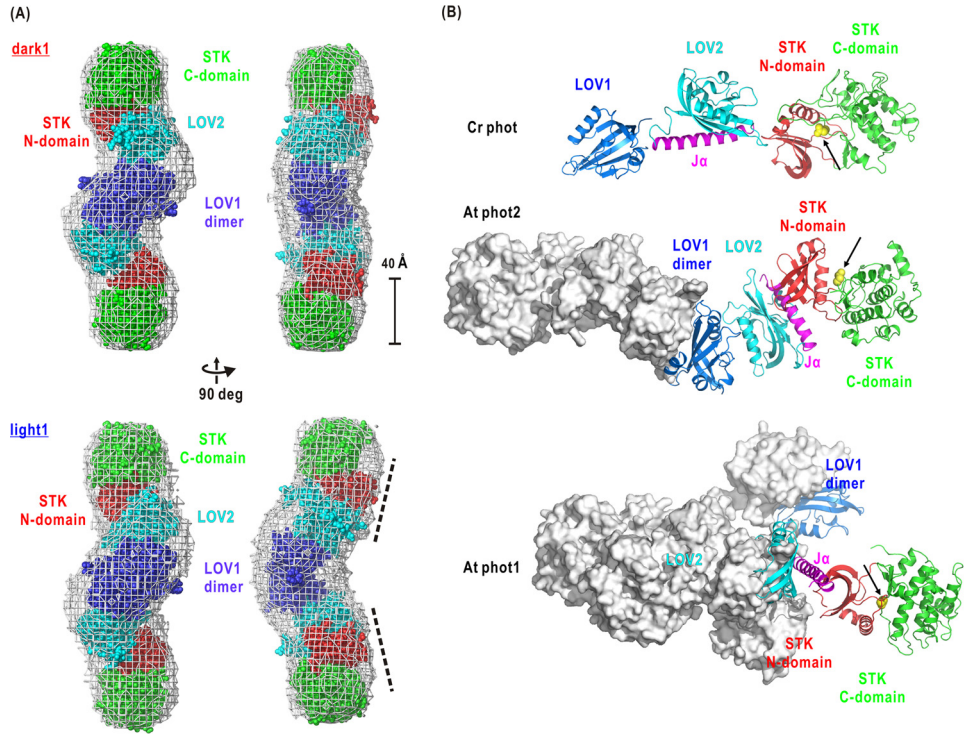

Figure 5. *A*, arrangement of the crystal structures of phot1 LOV1 (*blue*) (Protein Data Bank code 2Z6D), phot1 LOV2 (*cyan*) (Protein Data Bank code 4EEP), and the homology model of STK (N-domain (*red*) and C-domain (*green*)) in the molecular shapes (*white mesh*) of dark1 and light1. The homology model of STK was built from the crystal structure of cAMP-dependent protein kinase in the unliganded state (Protein Data Bank code 1J3H) as a template. In this arrangement, STK in one subunit could not easily contact the other subunit for intersubunit phosphorylation. *B*, comparison of putative models of Crphot, the Atphot1 dimer expected from the SAXS model for dimeric phot1 LOV2-STK, and the Atphot2 dimer from this study. In the models, the Jα regions are colored *purple*. The *arrows* indicate the side chains of the active-site aspartate residues illustrated as a space-filling model colored *purple*.

vitro assay (Fig. 1*E*), λPPase-treated WT was phosphorylated at a few sites under BL. This difference suggests that other factors accelerate phosphorylation, for instance a molecular complex with the partners of a kinase cascade *in vivo*. In the dark, phot2 was dephosphorylated by any phosphatase *in vivo* (36). Although the SAXS experiments were conducted for D720N mutant without phosphorylation, the structure and the BL-induced conformational changes would be similar to those of phot2 with a small number of phosphorylated residues *in vivo*.

Fig. 5*B* compares the expected molecular structures of Atphot1, Atphot2, and Crphot (25–27). Monomeric Crphot is thought to be located near the origin of the molecular evolution of phot (37). In land plants, phot2 is thought to be a prototype of phot and would be an origin of the diverse evolution to phot1 (38). Although Atphot2 forms a dimer by the association of LOV1, both LOV1 and LOV2 are involved in dimer formation in Atphot1. Therefore, the arrangement and association of LOV1 and LOV2 domains might become more complex in the course of evolution, in the order of Crphot, Atphot2, and Atphot1, and would be crucial for the functions of phot1 and phot2. A phot2 mutant with the LOV1 and LOV2 swapped from phot1 does not induce a normal dark positioning, which is a phot2-specific response in *Arabidopsis* (39). Based on the differences in the association modes between phot1 and phot2 dimers, the swapping may cause changes in the conformation and arrangement of LOV1 and LOV2, making it difficult for the swapped mutant to recognize the substrates, which is necessary to induce the dark positioning.

Functional roles of LOV1 in phot2

Currently, it is believed that for phot2 LOV2 is primarily responsible for the BL-induced conformational changes and that LOV1 only acts as a dimerization site and has little influence on the BL-dependent conformational changes that activate STK. From the present phosphorylation assay for C170A and C426A mutants (Fig. 1*E*), phosphorylation activity is likely dominated by LOV2. However, influences of LOV1 on the photocycle of LOV2 and the kinase activity have been reported. For instance, the C426A mutant of Atphot2 is reported to have kinase activity *in vitro* (19) and *in vivo* (31, 40). LOV2-STK of Atphot1 displays a reduction in the fluence-dependent response compared with the full-length protein *in vivo* (20). In Crphot, LOV1 contributes to increase the sensitivity of the fluence-dependent response (26). The dark reversion of LOV depends on the size of the LOV-containing fragment (16, 19).

The present study of the purified full-length phot2 revealed that, at the molecular level, BL-induced small conformational changes in LOV1 would influence the photocycle of LOV2 and vice versa (Fig. 2*E*). Therefore, LOV1 and probably its N- and C-terminal regions would play a role to produce the long-lived S_{390} of LOV2 that is advantageous to sustainably activate STK. In addition, the BL-dependent SAXS changes in C170A/D720N and C426A/D720A mutants were smaller than those of the D720N mutant. This result suggested that BL-induced LOV1 and LOV2 cooperatively contribute to BL-induced SAXS changes in the D720N mutant (Fig. 4*E*).

The BL-dependent phosphorylation of Ser-106 in λPPase-treated WT (Fig. 1*E*) may provide a clue to understand how the small conformational changes in LOV1 propagate to LOV2. As the N- and C-terminal regions in the α/β-scaffold of LOV1 are in close location, the conformational changes around Ser-106 near the N terminus of LOV1 may be transmitted to the linker region connecting the N and C termini of LOV2. In the case of phot1 LOV2-STK, the N- and C-terminal regions are critical for transmitting small conformational changes in LOV2 to STK (27, 28). In the next step to understand the molecular mechanism, it will be necessary to perform mutation analyses for the N- and C-terminal regions of LOV1.

Experimental procedures

Overexpression system

The full-length DNA fragment of Atphot2 was prepared with primers and the pGEX_phot2 as a template (30). Amplified DNA was inserted into the BamHI/XhoI site in the modified pET28a vector, the NdeI site of which was substituted by a BamHI site. To prepare mutants of full-length Atphot2, PCR-based mutagenesis was performed using PrimeStar GXL DNA polymerase (TaKaRa, Shiga, Japan) with primers. The following primers were used: 5′-GTTGGAAGAAACGCCCGGTTTC-TGCAA-3′ and 5′-TTGCAGAAACCGGGCGTTTCTTCC-AAC-3′ for the C179A mutation, 5′-TTGGGGAGAAATGC-CCGGTTTCTTCAG-3′ and 5′-CTGAAGAAACCGGGCAT-TTCTCCCCAA-3′ for the C426A mutation, and 5′-ATAGT-ATTGGCTAATTTTGATTTATCA-3′ and 5′-TGATAAAT-CAAAATTAGCCAATACTAT-3′ for the D470N mutation.

Each overexpression vector was transformed into *Escherichia coli* Rosetta2 (DE3) cells. Overexpression of the Atphot2 protein was induced by adding isopropyl 1-thio-β-D-galactopyranoside at a final concentration of 0.05 mM to the culture in the dark. Cells were harvested under a dim red light and stored at −80 °C until purification.

Purification

Purification was performed under a dim red light. Cells were freeze-thawed and suspended in a buffer containing 0.5 M NaCl, 10% (w/v) glycerol, and 20 mM HEPES-NaOH (pH 7.5). A protease inhibitor mixture (Roche Applied Science), Triton X-100 (final concentration of 1% (w/v)), and lysozyme (final concentration of 1 mg ml^{-1}) were then added to the suspension. After incubation on ice for 1 h, cells were lysed by sonication. The crude extract was centrifuged (100,000 × *g*, 30 min, 4 °C), and its supernatant was loaded onto a nickel-affinity column (His-Trap, GE Healthcare). Partially purified protein, which was eluted with a buffer containing 0.5 M imidazole, was purified further by SEC using a HiLoad 26/600 Superdex 200 prep grade (GE Healthcare) column equilibrated by a buffer containing 100 mM NaCl, 10% (w/v) glycerol, and 20 mM Tris-HCl (pH 7.8). Finally, fractions containing Atphot2 were loaded onto an anion-exchange column (Mono Q HR 5/5, GE Healthcare) and purified with a NaCl gradient. Fractions containing Atphot2 were concentrated using ultrafiltration (Amicon Ultra, Merck Millipore). The purity of the specimens was examined using SDS-PAGE after each column chromatography. The apparent molecular weight of Atphot2 was measured by SEC using a HiLoad 16/60 Superdex 200 prep grade (GE Healthcare) column equilibrated by a buffer containing 100 mM NaCl, 10% (w/v) glycerol, and 20 mM Tris-HCl (pH 7.8). For SAXS measurements and EM, Atphot2 was purified further by additional SEC using a buffer containing 20 mM Tris-HCl (pH 7.8), 500 mM NaCl, and 10% (w/v) glycerol.

Kinase assay

Kinase assays were performed as reported previously (41). An Atphot2 solution was incubated for 15 min at 20 °C in a kinase reaction buffer containing 100 mM NaCl, 10% (w/v) glycerol, 10 mM $MgCl_2$, 10 μM [γ-^{32}P]ATP (3.7 kBq μl^{-1}), and 20 mM Tris-HCl (pH 7.8). For blue-light excitation, a blue-light–emitting diode panel with an emission maximum at 475 nm (ISL-150X150-88, CCS Inc., Japan) was used. The reaction was stopped by boiling for 3 min after addition of SDS sample buffer. After SDS-PAGE of the specimens, the polyacrylamide gel was stained with Coomassie Brilliant Blue and dried. Phosphorylated bands were visualized using an imaging plate (Fujifilm) and a scanner (Storm, GE Healthcare). The signal intensities were measured using ImageJ software.

Mass spectrometry

In-gel digestions were performed as described previously (42). An LTQ-Orbitrap XL (Thermo Fisher Scientific) coupled with an EASY-nLC 1000 (Thermo Fisher Scientific) was used for nano-LC-tandem mass spectrometry (MS/MS) analyses as described previously (43). Mass Navigator version 1.3 (Mitsui Knowledge Industry) with the default parameters for the LTQ-Orbitrap XL was used to create peak lists on the basis of the recorded fragmentation spectra as described previously (44). Peptides were identified by using automated database searching with Mascot version 2.3.02 (Matrix Science) in The *Arabidopsis* Information Resource database (TAIR10_pep_20101214), which contains protein sequence information of His-tagged Atphot2 with a precursor mass tolerance of 3 ppm, a fragment ion mass tolerance of 0.8 Da, and strict trypsin specificity, allowing for up to two missed cleavages. Carbamidomethylation of Cys was set as a fixed modification, and oxidation of Met and phosphorylation of Ser, Thr, and Tyr were allowed as variable modifications. For quantitative analysis, MS peaks were detected using an in-house 2DICAL software package (45) that identified all MS/MS spectra using Mascot software, adjusted the retention times of each LC-MS data point utilizing the similarity index of the mass spectrum pattern, and grouped peaks from different samples that were derived from the same peptides in the direction of acquisition time. The peak intensities of the MS chromatograms were used as quantitative values.

Measurement of UV-visible absorption spectra

Absorption spectra and the time course of absorption changes in the dark reversion from S_{390} to D_{450} were measured at 293 K using a U-3100 spectrophotometer (Hitachi High-Technologies, Japan). The sample chamber was equipped with a 0305 thermostat controller (Hitachi High-Technologies) and was modified for measurements under continuous illumination by a BL-emitting diode with an emission maximum at 450 nm

(LUXEON star, Lumileds Lighting) (40). The procedures for measurements under irradiation of more than 200 μmol m^{-2} s^{-1} were reported previously (27). The specimens were dissolved in 20 mM Tris-HCl, 500 mM NaCl, 1 mM EDTA, and 10% (w/v) glycerol (pH 7.8). The reversion kinetics from S_{390} to D_{450} in the dark were monitored by the changes in absorption at 450 nm.

SAXS measurement

SAXS were collected at beamline BL45XU of SPring-8 using a PILATUS 300K-W detector (Dectris, Switzerland) as a series of 20 frames of 1-s exposures. The wavelength of the X-ray was tuned to 1.0000 Å. The camera distance was ~2500 mm. We used a single-specimen cell with quartz windows of 0.01-mm thickness and a path length of 3.0 mm. The temperature of the samples was maintained at 293 K.

Prior to the SAXS measurements, the specimen solutions were centrifuged at 15,000 × *g* for 1 h. Dynamic light scattering measurements confirmed that the supernatants were monodispersive. SAXS of D720N, C170A/D720N, C426A/D720N, and C170A/C426A/D720N mutants was collected in a concentration range from 0.5 to 1.2 mg ml^{-1}. For each specimen solution, three data were collected sequentially in the dark, under BL irradiation after a preirradiation of 2 min, and in the dark after 15-min dark reversion. Specimen solutions were irradiated using a light-emitting diode placed at 100-mm distance from the specimen position. The fluence rate at the specimen position was 450 μmol m^{-2} s^{-1}. Little radiation damage of all samples was confirmed by the stabilities in successively recorded SAXS profiles as well as by absorption spectra and SDS-PAGE patterns after the X-ray exposure. SAXS data of hen egg white lysozyme (apparent molecular weight of 14,300; Wako Chemical Industry, Osaka, Japan) was collected as a reference to estimate the apparent molecular weight of the D720N mutant.

SAXS analysis

One-dimensional SAXS profiles were reduced from the two-dimensionally recorded SAXS patterns after subtracting the background scattering from a buffer solution. Profiles in a very-small-angle region were analyzed by the Guinier approximation (46). Scattering intensity $I(S, C)$ at a scattering vector length S from a solution at a protein concentration C was approximated by the forward scattering intensity $I(S = 0, C)$ and $R_g(C)$ as follows,

$$I(S, C) = I(S = 0, C) \exp\left[-\frac{4\pi^2}{3} R_g(C)^2 S^2\right] \quad \text{(Eq. 1)}$$

$$S = \frac{2\sin\theta}{\lambda} \quad \text{(Eq. 2)}$$

where 2θ is the scattering angle and λ is the wavelength of the X-ray. For a dilute solution, the concentration dependences of $I(S, C)$ and $R_g(C)^2$ were approximated as follows,

$$\frac{KC}{I(S = 0, C)} = \frac{1}{M_w} + 2A{\cdot}C \quad \text{(Eq. 3)}$$

$$R_g(C)^2 = R_g(C = 0)^2 - B{\cdot}C \quad \text{(Eq. 4)}$$

where K is a constant. M_w is the apparent molecular weight of the protein. A and B are the second virial coefficient and a parameter reflecting the mode of intermolecular interactions, respectively (46). The sign of B is identical to that of A. Assuming a partial specific volume of 0.74 cm^3/g for soluble proteins, the apparent molecular weight of a target protein is estimated by comparing the $I(S = 0, C = 0)$ value with that of a reference protein (lysozyme) with a known apparent molecular weight. The distance-distribution function $P(r)$ was calculated using the program GNOM (47).

Molecular shape

The low-resolution molecular models of the D720N mutant in different states were restored as an assembly of small spheres of 3.8 Å, called dummy residues, using the program GASBOR (48), which minimizes the difference between experimental and calculated SAXS profiles under the constraints of maintaining a compact and interconnected arrangement of dummy residues. The difference in the observed ($I_{exp}(S)$) and model-calculated ($I_{model}(S)$) scattering profiles was monitored by the χ^2 value defined as follows,

$$\chi^2 = \frac{1}{N-1}\sum_{j=1}^{N}\left\{\frac{I_{exp}(S_j) - KI_{model}(S_j)}{\sigma(S_j)}\right\}^2 \quad \text{(Eq. 5)}$$

where N is the number of experimental data points. S_j is the scattering vector of the jth data point, K is a scale factor, and $\sigma(S_j)$ is the statistical error in the experimental scattering profile.

The χ^2 values depend on the number of dummy residues; therefore, we searched an optimum number of dummy residues giving the smallest χ^2 by varying the number from 800 to 1000 per subunit with a step of 25. For each number, 20 independent GASBOR calculations, starting from different models, were conducted, and then we found the optimum number (600 dummy residues per subunit). In the SAXS measurements, D720N and the other mutants were dissolved in 500 mM NaCl solution. Then the small electron density contrast between the D720N molecule and the solvent resulted in a smaller number of dummy residues than the number of amino acid residues. GASBOR calculations were performed for 576 different models for each state on a supercomputer system with 576 cores of Intel Xeon CPU X5690 (3.7 GHz per core).

After superimposing the 576 models as regards their moment of inertia, the distribution of dummy residues in each model was digitized in an assembly of 4 × 4 × 4-$Å^3$ voxels. Each model was then expressed as a point of multidimensional space spanned by the density in voxels. By principal component analysis, the distribution of molecular shapes in a multidimensional space was reduced onto the plane spanned by the first and second principal components. The models were then classified into 10 groups by K-means clustering after principal component analysis. Subsequently, we selected a molecular shape by averaging the models in the class composed of the largest number of models. The details of the analysis will be published

elsewhere.[3] Finally, the molecular shapes were expressed as density maps of the dummy residues in $4 \times 4 \times 4$-Å^3 cubes. The molecular models were illustrated using PyMOL (49).

Electron microscopy

A 3-μl solution of the C170A/C426A/D720N mutant was applied on a glow-discharged continuous carbon grid. The excess solution was removed using a filter paper, and the sample was subsequently stained on the carbon grid with 2% uranyl acetate. The negatively stained sample was observed using a JEM-1011 transmission electron microscope (JEOL, Japan) operated at 100 kV and equipped with an F114 slow-scan charge-coupled device camera (TVIPS, Germany) at a nominal magnification of 50,000×.

Author contributions—M. O., K. O., H. N., and M. N. data curation; M. O., K. O., H. N., T. K., Y. S., T. O., and M. N. formal analysis; M. O., K. O., T. O., and M. N. writing-review and editing; K. O. and M. N. conceptualization; K. O. and M. N. writing-original draft; T. K., T. H., and M. Y. methodology.

Acknowledgments—We are grateful to Professor Satoru Tokutomi of Osaka Prefecture University for encouragement and support in the preliminary stage of this study. We are grateful to Professor Keiichi Namba of Osaka University for EM of this study. The SAXS experiments were performed under the approval of the RIKEN Harima Institute (Proposals 2011007, 20140018, and 20150021).

References

1. Christie, J. M. (2007) Phototropin blue-light receptors. *Annu. Rev. Plant. Biol.* **58,** 21–45 CrossRef Medline
2. Petroutsos, D., Tokutsu, R., Maruyama, S., Flori, S., Greiner, A., Magneschi, L., Cusant, L., Kottke, T., Mittag, M., Hegemann, P., Finazzi, G., and Minagawa, J. (2016) A blue-light photoreceptor mediates the feedback regulation of photosynthesis. *Nature* **537,** 563–566 CrossRef Medline
3. Christie, J. M., Reymond, P., Powell, G. K., Bernasconi, P., Raibekas, A. A., Liscum, E., and Briggs, W. R. (1998) *Arabidopsis* NPH1: a flavoprotein with the properties of a photoreceptor for phototropism. *Science* **282,** 1698–1701 CrossRef Medline
4. Sakai, T., Kagawa, T., Kasahara, M., Swartz, T. E., Christie, J. M., Briggs, W. R., Wada, M., and Okada, K. (2001) *Arabidopsis* nph1 and npl1: blue light receptors that mediate both phototropism and chloroplast relocation. *Proc. Natl. Acad. Sci. U.S.A.* **98,** 6969–6974 CrossRef Medline
5. Kagawa, T., Sakai, T., Suetsugu, N., Oikawa, K., Ishiguro, S., Kato, T., Tabata, S., Okada, K., and Wada, M. (2001) *Arabidopsis* NPL1: a phototropin homolog controlling the chloroplast high-light avoidance response. *Science* **291,** 2138–2141 CrossRef Medline
6. Jarillo, J. A., Gabrys, H., Capel, J., Alonso, J. M., Ecker, J. R., and Cashmore, A. R. (2001) Phototropin-related NPL1 controls chloroplast relocation induced by blue light. *Nature* **410,** 952–954 CrossRef Medline
7. Kinoshita, T., Doi, M., Suetsugu, N., Kagawa, T., Wada, M., and Shimazaki, K. (2001) Phot1 and phot2 mediate blue light regulation of stomatal opening. *Nature* **414,** 656–660 CrossRef Medline
8. de Carbonnel, M., Davis, P., Roelfsema, M. R., Inoue, S., Schepens, I., Lariguet, P., Geisler, M., Shimazaki, K., Hangarter, R., and Fankhauser, C. (2010) The *Arabidopsis* PHYTOCHROME KINASE SUBSTRATE2 protein is a phototropin signaling element that regulates leaf flattening and leaf positioning. *Plant Physiol.* **152,** 1391–1405 CrossRef Medline
9. Möglich, A., Ayers, R. A., and Moffat, K. (2009) Structure and signaling mechanism of Per-ARNT-Sim domains. *Structure* **17,** 1282–1294 CrossRef Medline
10. Möglich, A., Yang, X., Ayers, R. A., and Moffat, K. (2010) Structure and function of plant photoreceptors. *Annu. Rev. Plant Biol.* **61,** 21–47 CrossRef Medline
11. Crosson, S., and Moffat, K. (2001) Structure of a flavin-binding plant photoreceptor domain: insights into light-mediated signal transduction. *Proc. Natl. Acad. Sci. U.S.A.* **98,** 2995–3000 CrossRef Medline
12. Crosson, S., and Moffat, K. (2002) Photoexcited structure of a plant photoreceptor domain reveals a light-driven molecular switch. *Plant Cell* **14,** 1067–1075 CrossRef Medline
13. Bögre, L., Okrész, L., Henriques, R., and Anthony, R. G. (2003) Growth signalling pathways in *Arabidopsis* and the AGC protein kinases. *Trends Plant Sci.* **8,** 424–431 CrossRef Medline
14. Salomon, M., Christie, J. M., Knieb, E., Lempert, U., and Briggs, W. R. (2000) Photochemical and mutational analysis of the FMN-binding domains of the plant blue light receptor, phototropin. *Biochemistry* **39,** 9401–9410 CrossRef Medline
15. Swartz, T. E., Corchnoy, S. B., Christie, J. M., Lewis, J. W., Szundi, I., Briggs, W. R., and Bogomolni, R. A. (2001) The photocycle of a flavin-binding domain of the blue light photoreceptor phototropin. *J. Biol. Chem.* **276,** 36493–36500 CrossRef Medline
16. Kasahara, M., Swartz, T. E., Olney, M. A., Onodera, A., Mochizuki, N., Fukuzawa, H., Asamizu, E., Tabata, S., Kanegae, H., Takano, M., Christie, J. M., Nagatani, A., and Briggs, W. R. (2002) Photochemical properties of the flavin mononucleotide-binding domains of the phototropins from *Arabidopsis*, rice, and *Chlamydomonas reinhardtii*. *Plant Physiol.* **129,** 762–773 CrossRef Medline
17. Iwata, T., Nozaki, D., Tokutomi, S., Kagawa, T., Wada, M., and Kandori, H. (2003) Light-induced structural changes in the LOV2 domain of *Adiantum* phytochrome3 studied by low-temperature FTIR and UV-visible spectroscopy. *Biochemistry* **42,** 8183–8191 CrossRef Medline
18. Okajima, K. (2016) Molecular mechanism of phototropin light signaling. *J. Plant Res.* **129,** 149–157 CrossRef Medline
19. Christie, J. M., Swartz, T. E., Bogomolni, R. A., and Briggs, W. R. (2002) Phototropin LOV domains exhibit distinct roles in regulating photoreceptor function. *Plant J.* **32,** 205–219 CrossRef Medline
20. Sullivan, S., Thomson, C. E., Lamont, D. J., Jones, M. A., and Christie, J. M. (2008) *In vivo* phosphorylation site mapping and functional characterization of *Arabidopsis* phototropin 1. *Mol. Plant* **1,** 178–194 CrossRef Medline
21. Harper, S. M., Neil, L. C., Day, I. J., Hore, P. J., and Gardner, K. H. (2004) Conformational changes in a photosensory LOV domain monitored by time-resolved NMR spectroscopy. *J. Am. Chem. Soc.* **126,** 3390–3391 CrossRef Medline
22. Christie, J. M., Yang, H., Richter, G. L., Sullivan, S., Thomson, C. E., Lin, J., Titapiwatanakun, B., Ennis, M., Kaiserli, E., Lee, O. R., Adamec, J., Peer, W. A., and Murphy, A. S. (2011) phot1 inhibition of ABCB19 primes lateral auxin fluxes in the shoot apex required for phototropism. *PLoS Biol.* **9,** e1001076 CrossRef Medline
23. Demarsy, E., Schepens, I., Okajima, K., Hersch, M., Bergmann, S., Christie, J., Shimazaki, K., Tokutomi, S., and Fankhauser, C. (2012) Phytochrome Kinase Substrate 4 is phosphorylated by the phototropin 1 photoreceptor. *EMBO J.* **31,** 3457–3467 CrossRef Medline
24. Takemiya, A., Sugiyama, N., Fujimoto, H., Tsutsumi, T., Yamauchi, S., Hiyama, A., Tada, Y., Christie, J. M., and Shimazaki, K. (2013) Phosphorylation of BLUS1 kinase by phototropins is a primary step in stomatal opening. *Nat. Commun.* **4,** 2094CrossRef Medline
25. Takayama, Y., Nakasako, M., Okajima, K., Iwata, A., Kashojiya, S., Matsui, Y., and Tokutomi, S. (2011) Light-induced movement of the LOV2 domain in an Asp720Asn mutant LOV2-kinase fragment of *Arabidopsis* phototropin 2. *Biochemistry* **50,** 1174–1183 CrossRef Medline
26. Okajima, K., Aihara, Y., Takayama, Y., Nakajima, M., Kashojiya, S., Hikima, T., Oroguchi, T., Kobayashi, A., Sekiguchi, Y., Yamamoto, M., Suzuki, T., Nagatani, A., Nakasako, M., and Tokutomi, S. (2014) Light-induced conformational changes of LOV1 (light oxygen voltage-sensing domain 1) and LOV2 relative to the kinase domain and regulation of

[3] M. Odie, Y. Sekiguchi, A. Fukuda, K. Okajima, T. Oroguchi, and M. Nakasako, manuscript in preparation.

kinase activity in *Chlamydomonas* phototropin. *J. Biol. Chem.* **289,** 413–422 CrossRef Medline

27. Oide, M., Okajima, K., Kashojiya, S., Takayama, Y., Oroguchi, T., Hikima, T., Yamamoto, M., and Nakasako, M. (2016) Blue light-excited light-oxygen-voltage-sensing domain 2 (LOV2) triggers a rearrangement of the kinase domain to induce phosphorylation activity in *Arabidopsis* phototropin1. *J. Biol. Chem.* **291,** 19975–19984 CrossRef Medline
28. Kashojiya, S., Okajima, K., Shimada, T., and Tokutomi, S. (2015) Essential role of the A′α/Aβ gap in the N-terminal upstream of LOV2 for the blue light signaling from LOV2 to kinase in *Arabidopsis* phototropin1, a plant blue light receptor. *PLoS One* **10,** e0124284 CrossRef Medline
29. Kashojiya, S., Yoshihara, S., Okajima, K., and Tokutomi, S. (2016) The linker between LOV2-Jα and STK plays an essential role in the kinase activation by blue light in *Arabidopsis* phototropin1, a plant blue light receptor. *FEBS Lett.* **590,** 139–147 CrossRef Medline
30. Okajima, K., Kashojiya, S., and Tokutomi, S. (2012) Photosensitivity of kinase activation by blue light involves the lifetime of a cysteinyl-flavin adduct intermediate, S390, in the photoreaction cycle of the LOV2 domain in phototropin, a plant blue light receptor. *J. Biol. Chem.* **287,** 40972–40981 CrossRef Medline
31. Suetsugu, N., Kong, S. G., Kasahara, M., and Wada, M. (2013) Both LOV1 and LOV2 domains of phototropin2 function as the photosensory domain for hypocotyl phototropic responses in *Arabidopsis thaliana* (Brassicaceae). *Am. J. Bot.* **100,** 60–69 CrossRef Medline
32. Inoue, S., Matsushita, T., Tomokiyo, Y., Matsumoto, M., Nakayama, K. I., Kinoshita, T., and Shimazaki, K. (2011) Functional analyses of the activation loop of phototropin2 in *Arabidopsis*. *Plant Physiol.* **156,** 117–128 CrossRef Medline
33. Nakasako, M., Zikihara, K., Matsuoka, D., Katsura, H., and Tokutomi, S. (2008) Structural basis of the LOV1 dimerization of *Arabidopsis* phototropins 1 and 2. *J. Mol. Biol.* **381,** 718–733 CrossRef Medline
34. Nakasako, M., Iwata, T., Matsuoka, D., and Tokutomi, S. (2004) Light-induced structural changes of LOV domain-containing polypeptides from *Arabidopsis* phototropin 1 and 2 studied by small-angle X-ray scattering. *Biochemistry* **43,** 14881–14890 CrossRef Medline
35. Christie, J. M., Hitomi, K., Arvai, A. S., Hartfield, K. A., Mettlen, M., Pratt, A. J., Tainer, J. A., and Getzoff, E. D. (2012) Structural tuning of the fluorescent protein iLOV for improved photostability. *J. Biol. Chem.* **287,** 22295–22304 CrossRef Medline
36. Tseng, T. S., and Briggs, W. R. (2010) The *Arabidopsis* rcn1–1 mutation impairs dephosphorylation of Phot2, resulting in enhanced blue light responses. *Plant Cell* **22,** 392–402 CrossRef Medline
37. Li, F. W., Rothfels, C. J., Melkonian, M., Villarreal, J. C., Stevenson, D. W., Graham, S. W., Wong, G. K., Mathews, S., and Pryer, K. M. (2015) The origin and evolution of phototropins. *Front. Plant Sci.* **6,** 637 CrossRef Medline
38. Galván-Ampudia, C. S., and Offringa, R. (2007) Plant evolution: AGC kinases tell the auxin tale. *Trends Plant Sci.* **12,** 541–547 CrossRef Medline
39. Aihara, Y., Tabata, R., Suzuki, T., Shimazaki, K., and Nagatani, A. (2008) Molecular basis of the functional specificities of phototropin 1 and 2. *Plant J.* **56,** 364–375 CrossRef Medline
40. Cho, H. Y., Tseng, T. S., Kaiserli, E., Sullivan, S., Christie, J. M., and Briggs, W. R. (2007) Physiological roles of the light, oxygen, or voltage domains of phototropin 1 and phototropin 2 in *Arabidopsis*. *Plant Physiol.* **143,** 517–529 CrossRef Medline
41. Okajima, K., Matsuoka, D., and Tokutomi, S. (2011) LOV2-linker-kinase phosphorylates LOV1-containing N-terminal polypeptide substrate via photoreaction of LOV2 in *Arabidopsis* phototropin1. *FEBS Lett.* **585,** 3391–3395 CrossRef Medline
42. Shevchenko, A., Tomas, H., Havlis, J., Olsen, J. V., and Mann, M. (2006) In-gel digestion for mass spectrometric characterization of proteins and proteomes. *Nat. Protoc.* **1,** 2856–2860 CrossRef Medline
43. Fujita, S., Pytela, J., Hotta, T., Kato, T., Hamada, T., Akamatsu, R., Ishida, Y., Kutsuna, N., Hasezawa, S., Nomura, Y., Nakagami, H., and Hashimoto, T. (2013) An atypical tubulin kinase mediates stress-induced microtubule depolymerization in *Arabidopsis*. *Curr. Biol.* **23,** 1969–1978 CrossRef Medline
44. Nakagami, H., Sugiyama, N., Mochida, K., Daudi, A., Yoshida, Y., Toyoda, T., Tomita, M., Ishihama, Y., and Shirasu, K. (2010) Large-scale comparative phosphoproteomics identifies conserved phosphorylation sites in plants. *Plant Physiol.* **153,** 1161–1174 CrossRef Medline
45. Ono, M., Shitashige, M., Honda, K., Isobe, T., Kuwabara, H., Matsuzuki, H., Hirohashi, S., and Yamada, T. (2006) Label-free quantitative proteomics using large peptide data sets generated by nanoflow liquid chromatography and mass spectrometry. *Mol. Cell. Proteomics* **5,** 1338–1347 CrossRef Medline
46. Guinier, A., and Fournet, G. (1955) *Small-Angle Scattering of X-rays*, Wiley, New York
47. Svergun, D. I. (1992) Determination of the regularization parameter in indirect-transform methods using perceptual criteria. *J. Appl. Crystallogr.* **25,** 495–503 CrossRef
48. Svergun, D. I., Petoukhov, M. V., and Koch, M. H. (2001) Determination of domain structure of proteins from X-ray solution scattering. *Biophys. J.* **80,** 2946–2953 CrossRef Medline
49. DeLano, W. L. (2012) *The PyMOL Molecular Graphics System*, Schrödinger, LLC, New York

Blue light–excited LOV1 and LOV2 domains cooperatively regulate the kinase activity of full-length phototropin2 from *Arabidopsis*

Mao Oide, Koji Okajima, Hirofumi Nakagami, Takayuki Kato, Yuki Sekiguchi, Tomotaka Oroguchi, Takaaki Hikima, Masaki Yamamoto and Masayoshi Nakasako

J. Biol. Chem. 2018, 293:963-972.
doi: 10.1074/jbc.RA117.000324 originally published online December 1, 2017